

## FEATURE ARTICLE

### A Quantum Chemical Approach to the Study of Reaction Mechanisms of Redox-Active Metalloenzymes

Margareta R. A. Blomberg\* and Per E. M. Siegbahn

*Department of Physics, Stockholm University, Box 6730, S-113 85 Stockholm, Sweden*

Reaction mechanisms of redox-active enzymes have for a long time been challenging targets for theoretical research. In this review, a quantum chemical approach will be described which during recent years has been applied in our laboratory to a number of the most interesting of these enzymes. Hybrid density functional theory is used where full geometry optimizations are done with a medium basis and final energies are evaluated using a much larger basis. Models consisting of 40–50 atoms and which contain the active site metal complex, including only the first-shell amino acid ligands, are normally employed. The protein surrounding is treated as a homogeneous dielectric medium. Results demonstrating the accuracy reached in this type of model are given, and a number of examples are described, showing the type of problems that can be treated. The most important of these are taken from studies on photosynthesis and oxidative phosphorylation (respiration).

#### I. Introduction

The study of mechanisms for redox-active metalloenzymes is one of the most exciting and active areas of chemistry today. This group of enzymes includes, for example, photosystem II of photosynthetic organisms, the terminal respiratory enzyme cytochrome oxidase, the nitrogen activating enzyme nitrogenase, the methane activating enzyme methane monooxygenase, ribonucleotide reductase, which converts ribonucleotides into deoxyribonucleotides, and many other enzymes of fundamental importance for life processes. Despite their obvious importance and the intense experimental interest, until a few years ago, there were only very few studies of these systems using accurate quantum chemical methods. The main reason for this is, of course, that the active sites of these enzymes are quite complex from an electronic structure viewpoint. The active metal cofactor of nitrogenase, for example, contains seven iron atoms and one molybdenum atom, and the oxygen evolving complex in photosystem II contains four manganese atoms. In the latter case, there is also the additional complication that the geometric structure is not yet known. A quantum chemical study of a reaction mechanism implies the determination of all intermediates and transition states along the reaction path. Transition states

may be difficult to locate already for small systems, and only a few years ago, this had hardly been done for systems larger than 20 atoms. Accurately determining the activation energy for a model of a complicated active site containing transition metal centers and more than 30 atoms, therefore, clearly represents a major challenge for computational chemistry. Despite these difficulties, during recent years, model calculations using accurate quantum chemical methods for the reaction mechanisms of these enzymes have started to become possible. The present review, which is not intended to give a general survey over the whole field, will describe an approach that has been used in our laboratory during the past five years to treat these complex systems. A brief description of the chemical model used in this approach is that, besides the substrate, it contains the active site metal complex, including all of its first-shell ligands. Examples from case studies will serve to illustrate what kind of questions that can be addressed and the level of understanding reached using this approach.

Calculations using high-accuracy methods on transition-metal-containing systems are relatively new. In the initial period, at the end of the 1980's, these calculations were restricted to very small systems containing less than 10 atoms. It turned out early

that it was very difficult to obtain qualitative agreement with experiments even for atoms unless very sophisticated methods and huge basis sets were used.<sup>1</sup> The reason was that both nondynamic and dynamic correlation effects are unusually large, and these effects are also strongly coupled. Still, after a few years of development, results could be obtained using a small degree of semiempirical parametrization,<sup>2</sup> which were in quite good agreement with experiments for small, mainly cationic, systems, for which accurate ion beam experiments were available.<sup>3–5</sup> A rather surprising experience from this period with model calculations on small systems, worth mentioning here since it was very important for the development of the present day models, was that even these small systems could provide insights which turned out to be generally relevant also for larger realistic systems. For example, insights obtained from studies of reactions between isolated transition metal atoms and alkanes<sup>6</sup> could be transferred to the understanding of the C–H activation of methane by systems used in homogeneous catalysis such as RhCp(CO).<sup>7</sup> The relative insensitivity of some of the most important results to the choice of model, for example, concerning the choice of ligands, was promising for future modeling of complex systems such as those in enzymes.

A breakthrough for the treatment of larger systems came with the development of highly accurate density functional methods about a decade ago.<sup>8</sup> The key to the increased accuracy of these methods was the incorporation of terms in the functionals that depend on the gradient of the density. This was primarily important for the description of the exchange energy,<sup>9</sup> much less so for the correlation energy.<sup>10</sup> Incorporation of exact exchange and a few semiempirical parameters were also significant in this context.<sup>11</sup> Benchmark calculations showed that using these so-called hybrid functionals, results almost as accurate as those obtained from the most accurate ab initio methods could be obtained at a fraction of the cost. For benchmark tests, which have gradually included more and more systems, the hybrid DFT methods have been shown to give energies normally within a few kilocalories per mole of essentially exact experiments. Even though this accuracy is surprisingly high, it must still be remembered that it cannot be expected that the error in a calculated barrier for an enzyme catalyzed reaction should be less than 3–5 kcal/mol. This limiting error is highly significant for the design of appropriately balanced methods and will be referred to several times in the present review.

With a limiting accuracy of 3–5 kcal/mol, it is clear that not all questions concerning reaction mechanisms can be meaningfully answered. Only the energetically most important aspects of the reaction mechanisms are therefore addressed. When two different reaction mechanisms are compared, the preferred mechanism can only be safely determined when there is an energetic difference between them of more than 3–5 kcal/mol. Fortunately, distinctly different mechanisms commonly differ by much more than this amount. For example, the activation mechanisms tried for O<sub>2</sub> cleavage in cytochrome oxidase differed by more than 15 kcal/mol,<sup>12,13</sup> as did some of the mechanisms for isopenicillin N synthase,<sup>14</sup> while the mechanisms tried in photosystem II<sup>15</sup> commonly differed by at least 5–10 kcal/mol. If two mechanisms investigated differ by less than 5 kcal/mol, the information provided could still be useful and could, together with experimental information sometimes, still be enough to decide upon the preferred mechanism, but in these cases, the energy information provided by the calculations is only of secondary importance. As a further clarification of the perspectives used here, two mechanisms which are geo-

metrically and energetically very similar and only have differences in the hydrogen bonding will in the present context be regarded as the same mechanism.

In the present review, the computational methods and models will be described first. Examples of accuracy will be given in this context. One of the major projects using this approach for oxygen activation by cytochrome oxidase will then be described with a comparison to the corresponding activation in isopenicillin N synthase. A discussion of the mechanism for hydroxylation in methane monooxygenase will serve to illustrate another type of questions that can be addressed with this approach, and finally, model calculations on the mechanism for O<sub>2</sub> formation in photosystem II will be described.

## II. Computational Methods and Models

In most quantum chemical studies on transition metal complexes in biological systems DFT methods are used. The obvious reason for this is the high efficiency of these methods for large systems. The particular functional chosen in the present approach is the B3LYP functional,<sup>11</sup> which is also the most widely used DFT method. In the first section below, the B3LYP method and its accuracy is discussed. To elucidate reaction mechanisms implies a large number of calculations, which means that for practical reasons the models used should be kept as small as possible. In the second section below, an investigation of the sensitivity of the calculated energetics to the size of the chemical models is discussed. In this context, more technical aspects, such as basis set and solvent effects on calculated energies, are also presented.

**II.A. Methods.** The hybrid B3LYP functional can be written as<sup>11,16</sup>

$$F^{\text{B3LYP}} = (1 - A)F_x^{\text{Slater}} + AF_x^{\text{HF}} + BF_x^{\text{Becke}} + CF_c^{\text{LYP}} + (1 - C)F_c^{\text{VWN}} \quad (1)$$

where  $F_x^{\text{Slater}}$  is the Slater exchange,  $F_x^{\text{HF}}$  is the Hartree–Fock exchange,  $F_x^{\text{Becke}}$  is the gradient part of the exchange functional of Becke,<sup>8</sup>  $F_c^{\text{LYP}}$  is the correlation functional of Lee, Yang, and Parr,<sup>17</sup> and  $F_c^{\text{VWN}}$  is the correlation functional of Vosko, Wilk, and Nusair.<sup>18</sup> The A, B, and C coefficients were determined<sup>11</sup> using a fit to experimental heats of formation, where the correlation functionals of Perdew and Wang<sup>19</sup> were used instead of  $F_c^{\text{VWN}}$  and  $F_c^{\text{LYP}}$  in the expression above.

The accuracy of different DFT methods has been investigated using the standard G2 benchmark test consisting of the enthalpies of formation of 148 small first and second row molecules.<sup>20</sup> These comparisons show that the B3LYP method is clearly superior to the other DFT methods, with an average deviation from experiments of only 3.11 kcal/mol.<sup>20</sup> This can be compared to the corresponding results of 1.58 and 0.94 kcal/mol, respectively, for the G2<sup>20</sup> and G3<sup>21</sup> methods, which are among the most accurate ab initio methods available. The accuracy of the B3LYP method has recently been further tested using the extended G3 benchmark set,<sup>22</sup> in which ionization potentials, electron affinities, and proton affinities also are included. This test has 376 entries, and the B3LYP functional obtains an average error of 4.27 kcal/mol.<sup>22</sup> The largest part of the increased error as compared to the previous benchmark comes from the inclusion of a new set of 75 enthalpies of formation for large molecules. However, enthalpies of formation for large molecules, where a large number of new bonds are formed, should be the least relevant when studying reaction mechanisms where only a few bonds are formed or broken, and

if this group is excluded, the B3LYP functional has an error of 3.29 kcal/mol (301 entries). For the geometries of a 55 atom subset of the G2 benchmark test, all DFT methods give quite accurate results, perhaps slightly more accurate for the hybrid methods.<sup>23</sup> The average B3LYP error for a bond distance in this benchmark is only 0.008 Å and for an angle only 0.61°. It is also worth noting that the geometry convergence with basis set is very fast.

Because of the lack of accurate experimental values, much less is known about the accuracy of DFT methods for transition metal complexes. The few systematic theoretical studies that have been performed were recently discussed in a review.<sup>24</sup> For small cationic systems, the average absolute error in calculated M–R bond energies, where M is a first row transition metal and R is H, CH<sub>3</sub>, CH<sub>2</sub>, or OH, were found to be in the range 3–5 kcal/mol using the B3LYP functional. For the successive M–CO bond energies in first transition row metal carbonyls, the average error was only 3 kcal/mol, and the results were in most cases within the experimental error bars. A comparison of particular interest for the present review also exists for the case of the O–H bond strength in MnO<sub>3</sub>(O–H)<sup>–</sup>,<sup>25</sup> where the B3LYP result was found to be in good agreement with experiment. This system is similar to the model systems discussed below for photosystem II.

When studying biochemical problems, it may be important to consider also the modeling of the part of the enzyme that surrounds the part treated quantum mechanically. For the present type of transition metal complexes, it has generally been found that effects coming from outside the metal complex are quite small. These are therefore reasonably well treated by simple continuum methods. The methods used in the applications discussed in this review employ cavities that follow the shapes of the molecular systems.<sup>26,27</sup> The dielectric constant of the protein is the main empirical parameter of this model, and in the studies discussed below, it was chosen to be equal to 4 in line with previous suggestions for proteins. This value corresponds to a dielectric constant of about 3 for the protein itself and 80 for the water medium surrounding the protein.

In the model studies discussed in the following sections, several calculations are performed for each structure considered. Initially, a geometry optimization is performed using the hybrid density functional B3LYP method.<sup>11</sup> In most cases, the geometry optimization is unconstrained, but recently, constrained optimizations have also been applied, where a few parameters are frozen to the corresponding values in the crystal structures. In this first step, standard double- $\zeta$  basis sets are used for all light elements. For the metals (manganese, iron and copper), a nonrelativistic effective core potential (ECP) is used. The valence basis set used in connection with this ECP (LANL2DZ)<sup>28</sup> is essentially of double- $\zeta$  quality. This basis set is used also for the Hessian calculations, i.e., second derivatives of the energy with respect to the nuclear coordinates, which are performed for the optimized structures, see further below. To evaluate relative energies, B3LYP calculations are further performed for the optimized geometries using larger basis sets, including diffuse functions and a single set of polarization functions on each atom. Finally, calculations of dielectric effects are performed in the optimized structures at the B3LYP level using the smaller basis set. The calculations are carried out using either the GAUSSIAN<sup>29</sup> or the JAGUAR program.<sup>30</sup>

In the investigation of reaction mechanisms, relative energies of intermediates and activation energies for the transitions between them have to be calculated. The activation energies are calculated as the energy difference between the reactant and

a transition state structure. A full transition state optimization requires the calculation of the Hessian. In most cases, approximate transition states are first determined by freezing one or two coordinates at different values, optimizing all the other degrees of freedom, and determining the maximum (or saddle point) on the potential energy surface. The main frozen parameters are different bond distances to be formed or split. A full transition state optimization, using an explicitly calculated Hessian, is then performed with the approximate transition state as a starting structure. It has turned out that the activation energies normally change by only a few kilocalories per mole going from the approximate transition states to the fully optimized ones. The calculated Hessians are also used to estimate zero-point, thermal, and entropy effects on the relative energies in the harmonic approximation. For this purpose, Hessians are calculated also for the corresponding reactant structures.

Concerning the reliability of the B3LYP method for calculating activation energies, it can be noted that for small model systems, it has been found that B3LYP tends to slightly underestimate the barriers for hydrogen transfer reactions by 2–3 kcal/mol.<sup>31</sup> On the other hand, for complicated reactions, like the ones where an O–O bond is formed or cleaved, it can be expected that in the transition state regions there are several states relatively close in energy. A single configuration method (like B3LYP) could then lead to a somewhat poorer description of the transition-state region than of the equilibrium region, which could lead to slightly too high barriers.

**II.B. Accuracy of the Model.** As indicated in the Introduction, the choice of model employed here to describe the active site in metallo-enzymes was reached on the basis of a large amount of initial experience obtained during the past decade for smaller systems. Even though the results were obviously found to be extremely sensitive to the choice of oxidation state of the metal, the sensitivity of many results to the choice of ligands was often found to be quite small. Even the difference between nitrogen or oxygen derived ligands was frequently not found to be very significant in light of the overall accuracy of the methods used (see above). In the earliest application of the present approach, for methane hydroxylation by methane monooxygenase (MMO),<sup>32</sup> the ligands were therefore all chosen to be oxygen derived for simplicity. The number of hydroxyl ligands were chosen to match the known oxidation state. In later applications, more realistic models of the ligands were used, normally including the side chain of the actual amino acids. In the present subsection, some results using this more recent type of modeling will be described for the case of the entire catalytic cycle of manganese catalase, where different variants of modeling the active site are compared. The comparisons discussed involve both the chemical and the computational model. It should be noted that for the sake of comparison of the models, it should not matter if the suggested catalytic cycle is indeed the correct one or not.

The eight suggested steps of the catalytic cycle for manganese catalase are shown schematically in Figure 1. These steps can be briefly described as follows:

Step 1: A water molecule bridging the two manganese centers in the Mn<sub>2</sub>(II,II) complex is being substituted by a hydrogen peroxide molecule. Step 2: The O–O bond of hydrogen peroxide is cleaved forming a hydroxyl radical and a bridging hydroxide. The manganese complex has the oxidation states Mn<sub>2</sub>(III,II) at the end of this step. The transition state is one of electron transfer from one of the manganese centers to the hydrogen peroxide. Step 3: A spin-transition and a proton

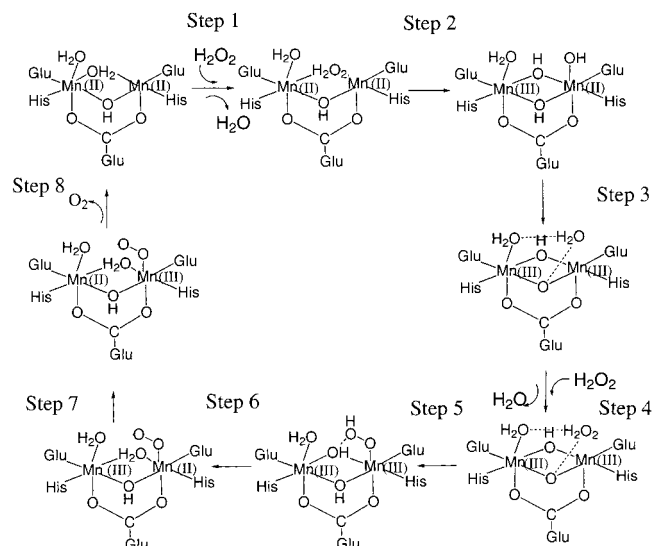


**Figure 1.** Schematic picture of the eight suggested steps of the catalytic cycle of manganese catalase.

transfer occur, leading to a  $\text{Mn}_2(\text{III},\text{III})$  complex with a bound water molecule. Step 4: The water molecule produced in Step 3 is substituted by a hydrogen peroxide molecule. The manganese complex is  $\text{Mn}_2(\text{III},\text{III})$ . Step 5: An O–H bond of the hydrogen peroxide that entered in Step 4 is heterolytically cleaved. The manganese complex remains in  $\text{Mn}_2(\text{III},\text{III})$ . Step 6: The second O–H bond of hydrogen peroxide is cleaved, leading to a terminally bound  $\text{O}_2$  ligand and a  $\text{Mn}_2(\text{III},\text{II})$  complex. The transition state is one of electron transfer from the peroxide to one of the manganese centers. Step 7: An electron is transferred between the manganese centers leading to a transfer from  $\text{Mn}_2(\text{III},\text{II})$  to  $\text{Mn}_2(\text{II},\text{II})$ . No transition state was obtained for this step. Step 8: A triplet oxygen molecule is being released.

Seven different models of varying size and accuracy were used to study this catalytic cycle, and the results were compared in a recent study on the model accuracy, where the details of the comparisons can be found.<sup>33</sup> The first model, which was described in the previous subsection and termed here as the standard model, is typical for the level of modeling and accuracy used in previous studies on metalloenzymes,<sup>12,14,15,24,34,35</sup> including the one on manganese catalase.<sup>36</sup> It uses as a chemical model the active site complex, including the first-shell ligands represented by their side chains only. For manganese catalase, this means using imidazoles for the histidines and formates for the glutamic acids. Computationally, it uses geometries optimized with a small double- $\zeta$  (DZ) basis set, and the energy in these geometries is obtained using a basis set where polarization and diffuse functions were added to all atoms. Zero-point vibrational effects are obtained from B3LYP Hessians with the DZ basis and are not varied in the investigations discussed below. The dielectric effects obtained using the SCI-PCM model<sup>27</sup> are finally added. The other models can be briefly described with relation to the standard model in the following way, where any aspect not mentioned are taken from the standard model. In the second model, the imidazoles are replaced by ammonia. In the third model, the formates are replaced by acetates. In the fourth model, the final energy is evaluated using the small DZ basis set. In the fifth model, on the other hand, the basis used for the final energy in the standard model is extended by a second set of polarization functions. The sixth model differs from the standard model in that the geometries are obtained at a higher accuracy by adding polarization functions to the DZ basis.

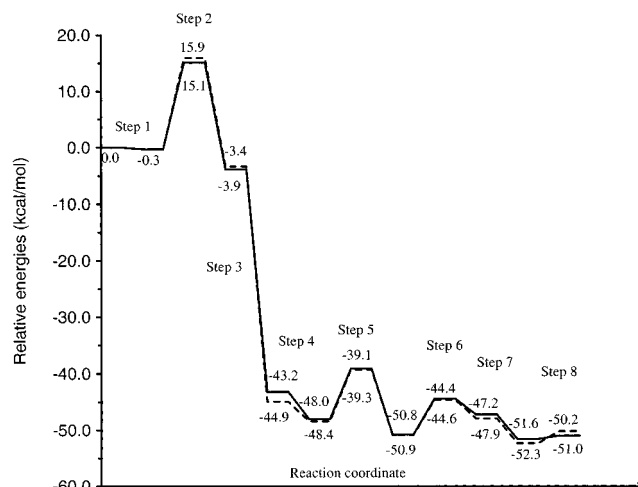


**Figure 2.** Energy diagram for the suggested mechanism of manganese catalase. The thick line represents the results using the standard model described in the text, where the geometries were optimized using a double- $\zeta$  basis, and the dashed line represents those with geometries obtained using a polarized basis.

Finally, in the seventh model, the dielectric effects are subtracted from the results of the standard model.

As a typical example of how a comparison between the different models appears for the entire catalytic cycle, the final energy diagrams for the standard model and for the model where a polarized basis set was used for the geometries are shown in Figure 2. The rate-limiting step is the second one, as expected, where the O–O bond of hydrogen peroxide is broken. After this, the resulting hydroxyl radical is immediately quenched in a strongly exothermic step. The barriers for the two subsequent O–H bond breaking reactions are relatively small, and triplet oxygen is easily released in the final step. It could be added that in a system like an enzyme, the kinetic energy released in one step is expected to be immediately quenched. The different steps in the mechanism should therefore be regarded as essentially dynamically independent. Thermodynamical equilibrium is assumed, and the rates of the individual steps should therefore be obtainable from the barrier heights reasonably accurately by applying transition state theory. The striking feature of the comparison in the figure is that the curves are very similar. For the barriers, the largest effect is in the rate-limiting second step with a difference of only 0.8 kcal/mol. It is clear that if two mechanisms are compared and the energy difference between these mechanisms is on the order of 10 kcal/mol, the effect of the improved geometry optimization does not affect the conclusions reached. This is in fact true also if the energy difference is small, less than 5 kcal/mol, since in this case a certain determination of the best mechanism can anyway not be made. In such a case, a conclusion concerning the preferred mechanism must rely heavily on experimental information. In summary, for systems like this, a geometry optimization using polarization functions is not needed for drawing a conclusion concerning the mechanism. This has been a general experience for all systems studied so far, and not a single counter-example has been discovered.

Comparisons similar to the one shown in Figure 2 were obtained for all the other models and the details can be found in the original study.<sup>33</sup> In the present review, only one more comparison will be discussed, and this is for the rate-limiting step of O–O bond cleavage and concerns all seven models. The conclusions drawn are essentially the same for all other steps of the mechanism. In this context, it should again be

remembered that B3LYP typically has an error of 3 kcal/mol. For all models except one, the result for the barrier falls within  $\pm 1$  of the result using the standard model, which is thus clearly within the error bars of the method. The only exception is the model where the final energy is evaluated using the small DZ basis set and where the error is 2.5 kcal/mol. Since the final energy evaluation does not represent a major part of the total computation time even with a polarized basis, it is clearly advisable to use at least this size of basis set for this part of the calculation. To add a second set of polarization functions for a system of the present size is not a major problem but has so far almost never resulted in a significant energy change. Very recent experience has shown that an extension of the basis set for the ECP in the 3s,3p region of the metal can sometimes have more important effects,<sup>37</sup> but this was not tried for manganese catalase. Exchanging the imidazoles in the standard model by ammonia does not have any significant effect on the barrier height, only 0.2 kcal/mol. This is true for all other steps except one in the catalytic cycle. In that step, the ammonia ligand forms an artificial hydrogen bond which cannot be formed by the actual histidine ligand or by the imidazole model. This type of effect is quite common in other systems and can in practice be the reason ammonia models cannot be used. The electronic structure effects of ammonia and imidazole are very similar even though ammonia lacks the conjugation present in imidazole. This similarity may be regarded as rather surprising, although it was in fact not surprising on the basis of the experience obtained from modeling smaller systems (see Introduction). It is perhaps less surprising that the results using formate and acetate ligands are so similar, with a difference on the barrier of only 0.4 kcal/mol, and this is true for all steps of the cycle. It should be added that the carboxylates are mechanistically important in many steps of the catalase cycle and change hydrogen bonding significantly. The glutamates can therefore not be modeled by ligands which lack the hydrogen bonding possibilities that carboxylates have.

The dielectric effects are very small on the rate-limiting barrier for manganese catalase, only  $-0.4$  kcal/mol. This is a rather common size, and effects larger than 3 kcal/mol are, in fact, quite unusual. Still, the evaluation of the dielectric effects is highly recommended first because they are obtained without a major effort and second because they can be rather large. In the cases when they turn out to be large, this is usually indicative of a problem in the chemical model chosen. For example, a highly significant hydrogen bond could be missing in the model. Since large dielectric effects tend to be uncertain, a recommendation in this situation is to extend the model rather than using the computed effect. A situation where the dielectric effects are large and cannot be easily modified by using a more realistic model is when there is a change of charge such as after an electron transfer. However, the use of continuum methods in those situations can only be expected to give results of qualitative accuracy, even though surprisingly accurate results have occasionally been found.<sup>38</sup>

When redox reactions are studied for transition metal complexes like those in catalase, it is usually much easier to obtain convergence for a ferromagnetic than for the proper antiferromagnetic coupling between the metal spins. Experimentally measured  $J$  values,<sup>39</sup> which tend to be small for systems like this, support this procedure. In the case of Mn-catalase, both solutions have recently been obtained for the O–O bond-cleavage step, and the difference in barrier height was found to be only 0.6 kcal/mol. It is not necessarily true that these effects always have to be small, and further research is necessary to settle this question. For example, when there are bridging sulfur

ligands like in nitrogenase,<sup>40,41</sup> it is our experience that the antiferromagnetic spin-coupling can be chemically more significant.

### III. Reaction Mechanisms

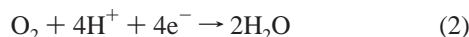
In this section, a few examples will be given of enzyme mechanisms studied recently to demonstrate what kinds of problems that can be addressed by quantum chemical methods. In the first section, common features of the O–O bond cleavage process in two quite different enzymes, cytochrome oxidase and isopenicillin N synthase, are discussed. In the second section, it is shown how quantum chemistry can provide new information that can be useful for determining the hydroxylation mechanism in methane monooxygenases, where different types of experiments have suggested quite different mechanisms. In the final section, several aspects of water oxidation in the plant enzyme photosystem II are discussed. The lack of crystal structure data for this important enzyme has made it particularly difficult to obtain the mechanism for the O<sub>2</sub> formation process.

**III.A. O–O Bond Cleavage Mechanism in Cytochrome Oxidase and Isopenicillin N Synthase.** Two enzymes which both cleave molecular oxygen will be discussed in this section. The entire catalytic cycles for these enzymes will not be discussed but, rather, one particular step, the cleavage of the O–O bond of the oxygen molecule. The purpose is to demonstrate that, by studying many different enzymes, similarities in the reaction mechanisms can be found, and thereby more general knowledge can be established. The two enzymes are cytochrome oxidase and isopenicillin N synthase.

Cytochrome oxidase is the terminal enzyme in the respiratory chain, located in the mitochondrial or the bacterial membrane in all aerobic organisms. The driving force of the respiratory electron transfer is the reduction of molecular oxygen to water, which occurs in cytochrome oxidase. The exergonic reduction of O<sub>2</sub> is coupled to proton translocation across the membrane, resulting in a proton gradient, which is used to produce ATP. The cytochrome oxidase enzyme has four metal centers, two copper centers, labeled Cu<sub>A</sub> and Cu<sub>B</sub>, and two heme iron centers, labeled heme a and heme a<sub>3</sub>. Two of these metal centers, Cu<sub>B</sub> and heme a<sub>3</sub>, located only about 5 Å apart (metal to metal distance) and therefore referred to as the binuclear center, constitute the active site for the O<sub>2</sub> activation process. The X-ray structures of both a mammalian<sup>42</sup> and a bacterial<sup>43</sup> cytochrome oxidase have been determined, and the structures around the binuclear center are found to be very similar for the two species, with three histidine ligands on Cu<sub>B</sub>. Although the experimental information on the cytochrome oxidase processes is very rich, the molecular details of the O<sub>2</sub> reduction process and the coupling to proton translocation are not very well understood.

Isopenicillin N synthase is a mononuclear non-heme iron enzyme that plays an important role for biosynthesis of antibiotics. By the use of one O<sub>2</sub> molecule, the enzyme catalyzes the bicyclic ring closure of the substrate  $\delta$ -(L- $\alpha$ -aminoadipoyl)-L-cysteinyl-D-valine (ACV) to form two water molecules and isopenicillin N, a precursor of the antibiotics penicillins and cephalosporins. Because of their outstanding importance in medicine, it is of interest to understand the mechanisms for formation of these antibiotics. The X-ray crystal structure has been obtained for isopenicillin N synthase of *Aspergillus nidulans*, complexed with manganese instead of iron. The crystal structure shows that the metal is octahedrally coordinated by two histidines, one aspartate, one glutamine, and two water molecules.<sup>44</sup>

The common reaction that occurs in these two enzymes is the O<sub>2</sub> reduction



In cytochrome oxidase, the electrons and protons are ultimately provided by the foodstuff metabolism in glycolysis and the citric acid cycle, and they are transported to the cytochrome oxidase enzyme via the respiratory chain enzymes. In isopencillin N synthase, the electrons and protons are more directly delivered by the ACV substrate, which needs to get rid of four hydrogen atoms to form the two rings of the isopencillin N product. The reactions taking place in the two enzymes are consequently very different. However, one similarity between the two enzymes is that the  $\text{O}_2$  molecule initially coordinates to an Fe(II) center, of heme type in cytochrome oxidase and non-heme type in isopencillin N synthase. Also, in the step that cleaves the O—O bond, an Fe(IV)=O center is formed in both cases. It is therefore possible to compare the mechanism for this particular reaction step of the two enzymes.

In cytochrome oxidase, the  $\text{O}_2$  molecule coordinates to the reduced form of the binuclear center, having the Fe(II) and Cu(I) oxidation states. To cleave the O—O bond requires four electrons. Two of these electrons are taken from iron, yielding the Fe(IV)=O product. At least one electron is taken from copper, yielding a Cu(II), and one of the main questions here is where the fourth electron comes from. One suggestion has been that it has to come from outside the binuclear center, i.e., from one of the other redox active metal centers, the heme a. This alternative is now more or less outruled, partly on the basis of the quantum chemical calculations. Other suggestions are that one more electron is taken from copper, yielding a Cu(III), or that the protein supplies this electron, yielding an amino acid radical. Spectroscopic data seems to outrule the formation of a porphyrin radical. The most likely amino acid candidate for providing an electron is the tyrosine residue, which has been found to be cross-linked to one of the histidines ligated to copper in the binuclear center.<sup>42,43</sup> Early calculations showed that an O—O bond cleavage with the formation of a tyrosine radical is thermodynamically favorable,<sup>12</sup> and more recent calculations indicate that this is more likely than the Cu(III) alternative.<sup>13</sup> There is also recent experimental evidence for the existence of a tyrosine radical in the O—O cleaved species.<sup>45</sup> The main question for a quantum chemical study is thus to elucidate how the O—O bond can be cleaved with a low enough barrier to be consistent with experimental data. The lifetime of the ferric oxy compound indicates that the free energy of activation should be about 13 kcal/mol.

For the mechanism involving the formation of a tyrosyl radical, it was originally proposed that the O—O bond is cleaved through a hydrogen atom transfer from the cross-linked tyrosine to the distal oxygen atom.<sup>46</sup> At the start of the theoretical study, it was noticed that a water molecule needs to be involved in this process, either as a link between the iron coordinated  $\text{O}_2$  molecule and tyrosine or as a copper coordinated proton source.<sup>13</sup> The latter alternative is the one discussed here, noting that the two versions of the O—O cleavage mechanism give very similar results.<sup>47</sup> In Figure 3a, the calculated potential surface for this mechanism is shown, and it can be seen that the barrier for the O—O bond cleavage is much too high, about 30 kcal/mol, as compared to the experimental value of 13 kcal/mol. The reason for this high barrier is a weak electronic coupling that is too weak between the tyrosine and the redox active iron center. However, if it is assumed that there is another proton available at the binuclear center, the O—O bond can be cleaved with a much lower barrier, calculated to be 14 kcal/mol, as shown in Figure 3b, and in excellent agreement with

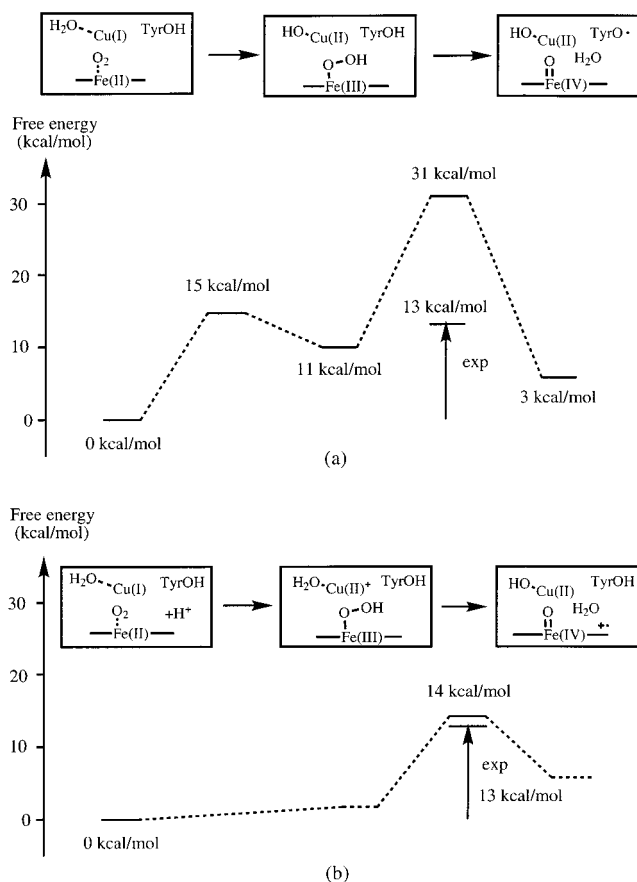


**Figure 3.** Calculated potential surfaces for O—O bond cleavage in cytochrome oxidase: (a) without an extra proton and (b) with an extra proton available at the binuclear center.

the experimental value for the rate-limiting barrier. There is in fact experimental evidence for such a protonation of the binuclear center during its reduction,<sup>48</sup> and it is suggested that the hydroxyl group at the farnesyl side chain of the heme  $a_3$  porphyrin is a likely site of the proton. This farnesyl hydroxyl group should have a high proton affinity due to resonances with the  $\pi$ -system of the heme ring,<sup>13</sup> and it is perfectly located, hydrogen-bonded to the cross-linked tyrosine and at the end of one of the proton channels.<sup>42,43</sup> In this mechanism, there is thus no tyrosine radical created in the actual O—O bond cleavage region of the potential surface. Instead, the calculations indicate the temporary formation of a porphyrin radical. As mentioned above, such a radical has not been observed, and it is therefore suggested that the radical is transferred from the heme to tyrosine in an exothermic step immediately following the O—O bond cleavage. The energetics for such a step is presently under investigation. In conclusion, the calculations have shown that in cytochrome oxidase the O—O bond cannot be cleaved with a reasonably low activation energy unless there is an extra proton present at the binuclear center.

In isopencillin N synthase, it has been shown that in the presence of the substrate ACV the glutamine loses its coordination to iron and is replaced by the thiolate of ACV. On the basis of substrate analogues and isotopic labeling experiments, a catalytic mechanism was first proposed by Baldwin et al.<sup>49,50</sup> Additional experimental data, giving a more detailed picture of the enzyme mechanism, have been gathered in three recent reviews.<sup>51–53</sup> The binding of the substrate and molecular oxygen into the enzyme leads to loss of one water molecule. In the subsequent step, the Cys- $\beta$ -C—H hydrogen of ACV migrates

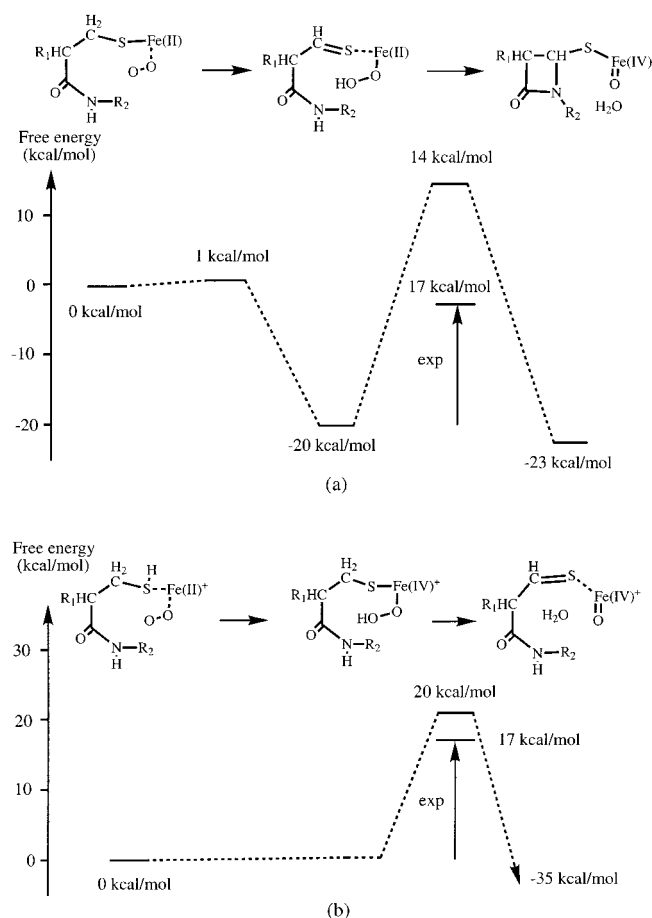


**Figure 4.** Calculated potential surfaces for O–O bond cleavage in isopenicillin N synthase: (a) with the substrate deprotonated and (b) with the substrate remaining protonated.

to the dioxygen, leading to formation of the oxoferryl and the  $\beta$ -lactam ring intermediate and a second water molecule. Spectroscopic<sup>49,50</sup> and crystallographic<sup>54</sup> studies have indicated that the closure of the  $\beta$ -lactam ring occurs prior to that of the thiazolidine ring, which completes the formation of the bicyclic structure of isopenicillin N. Furthermore, isotope labeling experiments show that kinetic isotope effects are present both for the Cys- $\beta$ -C–H hydrogen and for the Val- $\beta$ -C–H hydrogen, indicating that rate-determining C–H activations occur at these two sites.<sup>49</sup> Both steps should therefore have significant reaction barriers of similar size, around 17 kcal/mol.

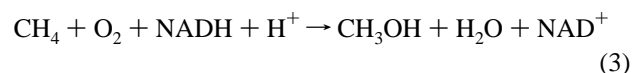
The first part of the catalytic cycle, the formation of the  $\beta$ -lactam ring and the cleavage of the O–O bond, will be discussed here. In the first set of calculations, the ACV substrate thiolate was assumed to be deprotonated when it coordinates to the iron center. The first step of the reaction would then be the hydrogen atom abstraction from Cys- $\beta$  carbon to the molecular oxygen. As shown in Figure 4a, this step turns out to have a very low barrier of only about 1 kcal/mol, which is thus in contradiction with the experimental observation that this should be one of the rate-limiting steps. Furthermore, the next step, which involves both the O–O bond cleavage and the  $\beta$ -lactam ring closure, is calculated to have a barrier of about 34 kcal/mol, as is also shown in Figure 4a, which is much too high compared to the experimental activation energy of only about 17 kcal/mol. Inspired by the results for cytochrome oxidase, the presence of one more proton at the active site was then studied, since this might reduce the O–O bond cleavage barrier. In this investigation, it was assumed that the ACV

substrate thiolate is still protonated upon coordination to the iron center. In fact, in the crystal structure the two oxygen ligands at the metal center have the same Fe–O bond distances, indicating that they are both water molecules and that the iron center has to carry one positive charge to give an Fe(II) oxidation state. This also means that the substrate does not have to become deprotonated when it replaces one of the water molecules as a ligand to iron. In the first step, the thiolate proton is transferred to molecular oxygen coordinated to iron forming an Fe–OOH peroxide structure (see Figure 4b). This step is assumed to be close to thermoneutral. In the next step, the hydrogen atom is transferred from the Cys- $\beta$  carbon, and the O–O bond is cleaved, with a calculated activation energy of 20 kcal/mol, in reasonable agreement with the experimental observations. The formation of the  $\beta$ -lactam ring occurs in a subsequent step, which was shown to have a low activation energy.<sup>14</sup>

Thus, the calculations have shown that for cytochrome oxidase and isopenicillin N synthase, in a very similar way, an extra proton is needed in the active site to allow O–O bond cleavage with a low enough barrier. In cytochrome oxidase, there is experimental evidence for protonation of the active site prior to the entrance of the O<sub>2</sub> molecule, and in isopenicillin N synthase, the crystal structure indicates that the substrate replaces a water molecule at the iron center, which makes it likely for the substrate to remain protonated at the thiolate group when coordinating to iron.

O–O bond cleavage of the oxygen molecule does not always have to occur through a heterolytic mechanism as in the above cases. Model calculations on methane monooxygenase have shown that a homolytic splitting appears more likely for this enzyme.<sup>34</sup> In the optimized transition state, the oxygen molecule is symmetrically oriented between the irons with the O–O bond perpendicular to the Fe–Fe bond. The reactant peroxide is in an Fe<sub>2</sub>(III,III) state and goes to an initial Fe<sub>2</sub>(III,IV) product as the O–O bond is cleaved through a donation of a single electron from one of the irons to oxygen. The transition state is thus one of electron transfer and strongly couples the O–O stretching to the Fe–O distances of the iron center that changes oxidation state in this reaction. Ferro- and antiferromagnetic couplings of the iron spins give a very similar description of this process.

**III.B. Hydrocarbon Hydroxylation in MMO.** Methane monooxygenases (MMOs) are a group of enzymes which convert methane to methanol via a monooxygenase pathway in which the dioxygen molecule is activated.<sup>51,53,55,56</sup> The overall reaction is given by



The longest known MMOs are soluble proteins containing a binuclear iron active site in the MMOH protein. The X-ray structure of MMOH with a diferric complex shows that there are two histidines, four glutamates, one terminal water, and two bridging oxygen derived ligands<sup>57</sup> (see Figure 5).

Although there are many interesting mechanistical aspects in MMO, in the present review, only the hydroxylation step will be discussed. The hydroxylation of hydrocarbons by MMO has been studied extensively experimentally and several possible mechanisms have been suggested.<sup>51,55</sup> In these mechanisms, compound **Q**, where the iron dimer is in an Fe<sub>2</sub>(IV,IV) state, is the hydroxylating species. The mechanisms fall into essentially two categories, radical and nonradical mechanisms. In the radical mechanism, the first step is a hydrogen abstraction from the hydrocarbon, and the second step is a recombination between the radical and the hydroxyl group. The nonradical mechanisms

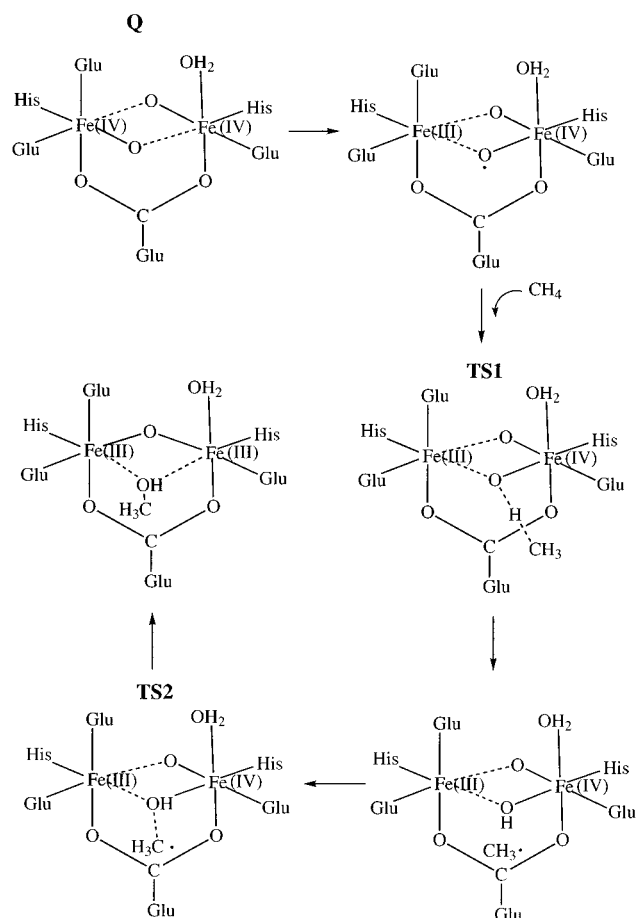


**Figure 5.** Suggested reaction sequence for hydroxylation in methane monooxygenase.

suggest a concerted insertion pathway. Support for the hydrogen abstraction mechanism comes from measurements by Lipscomb and co-workers,<sup>55</sup> who found some of the largest kinetic isotope effects (KIEs) ever observed in biology. Furthermore, radical spin trap experiments have detected radical species which were able to diffuse out of the protein matrix during the MMO reactions.<sup>58</sup> Support for a concerted nonradical mechanism of MMO comes mainly from radical clock measurements by Newcomb, Lippard, and co-workers.<sup>59</sup> In these experiments, radical clocks containing, for example, a cyclopropane ring, are constructed to have the property that if a hydrogen abstraction occurs the cyclopropane ring will open with a very high rate. When this happens, the product radical will move to one of the corners of the now open ring and will by strong preference be hydroxylated in this position. If there is hydrogen abstraction, the product alcohol should thus be ring-opened. However, in the experiments on both MMO and P-450, essentially only ring-closed products are found. For *Methylobacter capsulatus*, very fast radical clocks were studied with results interpreted to show a maximum radical lifetime as short as  $10^{-14}$ s. With these short lifetimes, the presence of radicals as intermediates in the hydroxylation was excluded, both for MMO and P-450.

The first B3LYP study of MMO found a very pure hydrogen abstraction transition state for methane activation.<sup>32</sup> In the second study, the mechanism was reinvestigated, but again, the same type of transition state was found.<sup>34</sup> In that study, the geometry was also systematically modified to approach a possible insertion transition state by bending the C–H–O angle, but the energy just increased rather steeply. A third study by Morokuma et al. performed in the meantime also gave the same

mechanism.<sup>60</sup> Apart from some studies on rather small and charged models, the results from the theoretical investigations therefore quite conclusively point toward a radical mechanism. It is very unlikely that the use of even larger models is going to change this situation. The solution to the problem of the drastic discrepancy between theoretical studies and the interpretation of the results of radical clock experiments therefore probably has to be sought somewhere else. A suggested solution was made in a recent study,<sup>61</sup> and this will be briefly described here, as another illustration of the type of problems that can be effectively attacked by theoretical methods.

For methane, which is the natural substrate for MMO, calculations have shown<sup>34,60</sup> that there is, besides the hydrogen abstraction transition state TS1, an additional transition state before the product alcohol is reached, TS2 in Figure 5. Calculations further show that TS1 is very similar for methane and the unsubstituted radical clock, with a pure hydrogen abstraction in both cases. In the second step, an electron transfer is involved, from the methyl radical formed in the first step, to the iron dimer complex. It is clear that the ionization potential of the substrate radical should be important for the size of this barrier. Indeed, the calculations show that for the radical clock substrates used in the experiments, which have substantially lower ionization potentials than methane, the barrier for this step disappears. The calculated gas phase ionization potential is 229 kcal/mol for methane and only 151 kcal/mol for the cyclopropane radical clocks. This difference will decrease in the enzyme but will remain large. It is therefore suggested that the radical clock substrate radicals will be ionized before the alcohol recombination occurs. If this happens reasonably fast after the hydrogen abstraction TS, calculations show that the unsubstituted cyclopropane clock cation will never open and only closed products will therefore be formed. For the phenyl-substituted clock, the situation is slightly more complex since the ring of the cation will open anyway with almost no barrier. A ring-opening can thus not be prevented in this case. To investigate what happens in this situation, an already fully optimized ring-opened radical clock cation (with a vinyl substituent, analogous to phenyl) was placed at the position of the methyl radical in the geometry for the methane transition state TS2 (see Figure 6). The subsequent geometry optimization led to an immediate ring closing of the clock and a formation of the alcohol at the methyl position without any barrier. Alcohols with closed cyclopropane rings could thus form even if a ring-opened radical is formed after the first step, in contrast to the normal interpretation of these experiments. This possibility represents one scenario which would resolve the discrepancy between theory and experiments. Another possibility, which would also resolve the problem, is that for the easily ionizable radical clocks with phenyl substituents, there is in fact a concerted transition state with a hydride transfer from the substrate to the bridging oxygen. An investigation of this possibility, which is in line with the normal interpretation of the experiments, is still under investigation and remains quite probable for the phenyl-substituted clocks. However, as mentioned above, this possibility does not apply for methane, which is the normal substrate for MMO and which therefore can be concluded to be activated via a radical mechanism.

**III.C. Water Oxidation in Photosystem II.** To determine the mechanism for the formation of an oxygen molecule from water by the oxygen-evolving center of photosystem II in green plants is one of the largest challenges in chemistry today. Despite decades of experimental studies, there are still large uncertainties concerning the detailed chemical steps of the water oxidizing

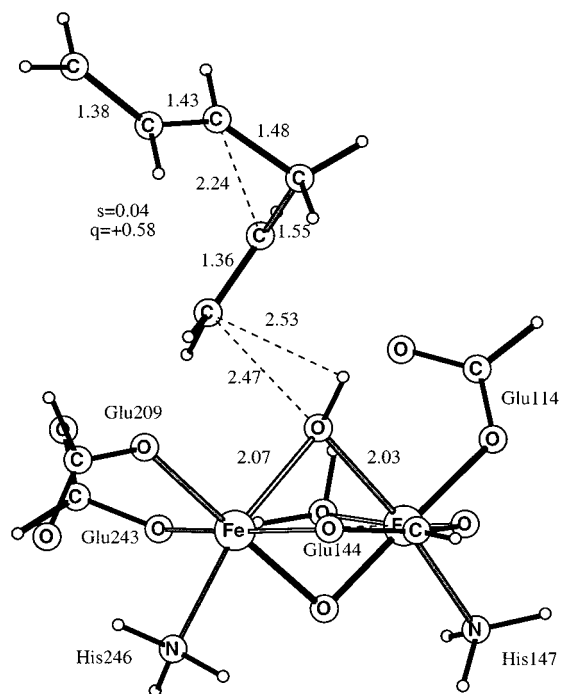


**Figure 6.** Starting structure for geometry optimization with an optimized ring-opened cationic clock and the iron dimer complex of MMO taken from the second TS structure for methane. The starting C–O distance was set to 2.47 Å and the C–H distance to 2.53 Å. This structure converged without any barrier to the alcohol product with a closed cyclopropane ring.

reactions. A major problem in this context is that the X-ray structure of the enzyme has not yet been obtained. Another problem is that the chemistry of these steps is so unique that it is very hard to find laboratory model reactions with any higher degree of similarity to water oxidation. With this background, theory could be helpful and provide pieces of information which cannot at present be obtained from experiments. Although the structure of the water oxidizing complex is not known, sufficient information from EXAFS is available<sup>62</sup> to start model calculations. This technique allows the description of the structural environment around the metals, due to its ability to deal with the local order around a relatively heavy atom (not H, C, N, O, ...).

From saturating flash experiments, water oxidation is known to occur in four steps.<sup>63</sup> The intermediates of these steps are denoted  $S_0$  through  $S_4$ , and  $O_2$  formation occurs at  $S_4$ . In each step, a photon is absorbed by the antenna pigments of the light-harvesting proteins, and the energy is transferred to the photosynthetic reaction centers of photosystems I and II. At the reaction center of photosystem II, a charge separation takes place, in which the chlorophyll P680 is ionized.  $P680^+$  is reduced by an electron coming from a tyrosine,  $Tyr_Z$  (Tyr161), located in the proximity of the water oxidizing complex.<sup>64</sup> In this process,  $Tyr_Z$  loses a proton to become a neutral tyrosyl radical. In some way,  $Tyr_Z$  is recreated by receiving an electron and a proton in each step of water oxidation. Two leading models for recreation of  $Tyr_Z$  exist. In the first model, termed the hydrogen abstraction mechanism<sup>65</sup> (see Figure 7a), the tyrosyl radical obtains both the proton and the electron from the manganese complex in a concerted hydrogen atom transfer step. In the second, model termed the electron transfer model (see Figure 7b), the tyrosyl radical obtains the electron from the manganese complex and the proton from a nearby base. In that model, the water molecules which will eventually form  $O_2$

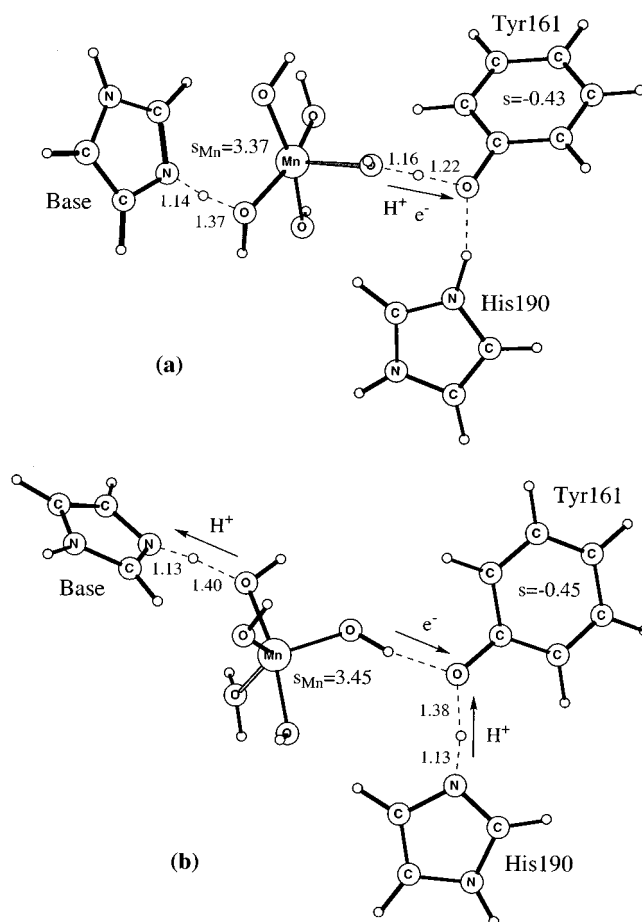


**Figure 7.** Optimized transition states for two models of tyrosine reduction in photosystem II: (a) the hydrogen atom transfer model and (b) the electron-transfer model.

will lose their protons to a different base.<sup>66</sup> It is very important to note that, independently of the mechanism of this process, the energy available to the water oxidizing complex in each step is approximately equal to the bond strength of the  $Tyr_Z$  O–H bond, which is equal to 87 kcal/mol. In other words, the O–H bond strength of the ligand bound to manganese has to be at most this amount.

The most critical part in the search for a possible water oxidation mechanism is to find O–H bond strengths close to the one of 87 kcal/mol in tyrosine so that a proton and an electron can be released according to one of the schemes in Figure 7. It should in this context be noted that the O–H bond strength of unligated water is as high as 118 kcal/mol. In the first theoretical study on this problem,<sup>67</sup> it was shown that the coordination of water and hydroxyl ligands to the manganese cluster indeed significantly lowers the O–H bond strengths of both water and hydroxide ligands, which is clearly one of the main functions of manganese in the water oxidation process. In these processes, manganese was first oxidized from Mn(III)–water to Mn(IV)–hydroxide and then further to Mn(V)–oxo, and the bond strengths were in both cases found to be close to the required value. However, only five-coordinated structures where the terminal ligands were water and hydroxide were used in the first study, and later studies have shown that the situation is somewhat more complicated than initially anticipated. Even a small modification, such as placing a water ligand in the second shell, leads to a significant increase of the O–H bond strength of the first-shell hydroxide ligand. In fact, so far, no realistic manganese complex has been found in these theoretical

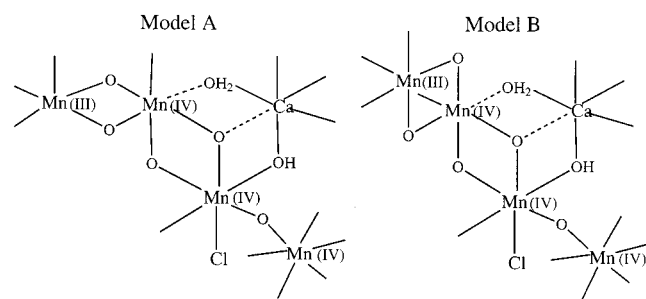


**Figure 8.** The two models of the water oxidizing cluster discussed in the text.

studies that can yield a terminal manganese-oxo state with a sufficiently low energy.<sup>15</sup> These results parallel the experimental findings, and at present, the general view is that terminal oxo ligands are not involved in the water oxidation process.

In a recent B3LYP modeling study of the water oxidation mechanism, quite realistic models of the water oxidation complex were used.<sup>15</sup> These models were constructed on the basis of available experimental information mainly from EXAFS and EPR and contain three tightly bound manganese centers and a calcium center with two short distances to manganese centers. No position could as yet be suggested for the fourth, less tightly bound manganese center, and this center was therefore left out of the model calculations. Two types of models fulfill the energetic requirements discussed above and also most of the geometric requirements set by EXAFS, and these models are shown in Figure 8, where the fourth manganese is tentatively added in the lower right corner. The key feature of the water oxidation mechanism found using these models is that a bridging oxygen radical is formed in the  $S_3$  state in the position below the upper Mn(IV) in the figure. The presence of an oxygen radical was also the main feature of an earlier study of the mechanism using a simpler model.<sup>68</sup> The creation of an oxygen radical in the  $S_2$ -to- $S_3$  transition means that manganese is not oxidized in this transition, which is in line with several previous suggestions based on XANES,<sup>62</sup> EPR,<sup>69</sup> and NMR<sup>70</sup> experiments. The model complexes in the figure contain a central cube with an empty corner, and it is suggested that the essential chemistry occurs in this cube. In the  $S_1$  state, the corners of the cube are formed by two Mn, one Ca, two  $\mu$ -oxo, and two waters. Water-oxidation is suggested to occur by removing protons from the two waters and from a  $\mu$ -hydroxo group. Calcium has an important chelating role in these processes and makes the O-H bonds sufficiently weak for the abstraction chemistry by the tyrosyl radical. In the suggested mechanism for the formation of the O-O bond in the  $S_4$  state, an external water molecule enters the originally empty corner of the cube. This water loses a hydrogen atom to the oxyl radical and then forms an O-O bond to an hydroxyl group bridging manganese and calcium. Simultaneously, a proton moves to a bridging hydroxyl group in another corner of the cube. At this point, the final  $H^+, e^-$  transfer to the tyrosyl radical occurs, a water molecule enters, and  $O_2$  is released. This mechanism is consistent with recent important solvent exchange experiments by Messinger et al.<sup>71</sup> who used labeled oxygens. In those experiments, the O-O bond was shown to be formed from one oxygen that is quickly exchanging with solvent water and one that is more slowly exchanging. The fast exchanging oxygen should come from the external water and the slow exchanging oxygen from the bridging hydroxyl group.

Finally, the reduction of the tyrosyl radical by the manganese complex has recently been studied using a simple mono-

nuclear complex with only water and hydroxyl ligands.<sup>72</sup> In the  $S_1$ -to- $S_2$  step, manganese is considered to be oxidized from Mn(III) to Mn(IV). To model this step, an  $Mn(III)(H_2O)_2(OH)_3$  complex is used (see Figure 7). Tyr<sub>Z</sub> (Tyr161) is modeled by a phenol group, and the base near Tyr<sub>Z</sub>, believed to be His190, is modeled by an imidazole group. This imidazole is protonated for the reactant of this reaction step, as a result of the proton transfer from tyrosine occurring upon its ionization. To be able to compare the two different mechanisms for the reduction of the tyrosyl radical discussed above, hydrogen atom transfer and electron transfer, an additional base (imidazole) was also included. An optimized transition state for a hydrogen atom transfer mechanism is shown in Figure 7a. As can be seen from this structure, a proton is halfway between a manganese ligated water and the tyrosyl group, and the spin populations, 3.37 on manganese and 0.43 on tyrosine, indicate that the electron is also halfway between manganese and tyrosine. (Mn(III) has a typical spin population of 2.9, and Mn(IV) has 3.9.) The calculated free energy of activation for this mechanism is 10.6 kcal/mol, in good agreement with a barrier of 12 kcal/mol as derived from the lifetime of the  $S_1$  state. An optimized transition state for an electron transfer mechanism is shown in Figure 7b, where the spin populations, 3.45 for manganese and 0.45 for tyrosine, clearly indicate that the electron is on its way between manganese and tyrosine. It can further be seen from the structure in this figure that a proton is moving from the imidazole modeling His190 to recreate a neutral tyrosine and that a proton is leaving the manganese complex to the other base. The calculations give a value of 17.5 kcal/mol for the free energy of activation for this mechanism. This value should be considered as preliminary, since more investigations are needed, e.g., concerning the best way to model this type of mechanism, but at this stage the calculated results indicate that the electron-transfer mechanism might be less favorable than hydrogen atom transfer.

#### IV. Conclusions

In the present review, a theoretical model for studying mechanisms of redox-active enzymes has been described. The model can be briefly described as containing the substrate and the active metal complex, including only its first-shell ligands, although in a few studies some second shell ligands have also been included. Computationally, the B3LYP method is used with geometries optimized using moderate basis sets, while the energies are obtained using large basis sets. Effects from the protein environment are obtained using continuum methods. One major advantage with this rather simple model is that it allows straightforward applications on a large number of enzymes and of many alternative mechanisms. Experience has shown that many different alternatives and many years of research with repeated investigations are usually required until consensus is reached for an enzyme mechanism.

In the text above, some typical examples of mechanistic studies have been described. Several other enzymes have also been studied using the same approach. One of the earliest applications was made to elucidate the mechanism for ammonia synthesis in nitrogenase.<sup>73</sup> A model including all steps from  $N_2$  to ammonia was set up where a coupled transfer of an electron and a proton to  $N_2$  in each step is a key factor. Another similar study was made for tyrosinase.<sup>74</sup> In both these studies, even simpler models than those described here were used, and work is in progress using more realistic models. Another enzyme thoroughly studied is NiFe-hydrogenase.<sup>76</sup> In the most recent modeling of this enzyme, which is still in progress, four second-shell ligands were included, two of them charged. When second-

shell ligands are included, these may have to be held in place somehow, and in this case, this was made simply by locking a position for each residue to its position from the crystallographic structure. A similar procedure was also used in a study of thermolysin, which is a zinc-containing peptidase.<sup>77</sup> For galactose oxidase, which oxidizes alcohols to aldehydes, a combined QM-MM procedure was used to include the peptide bridge between two of the ligands of copper.<sup>35</sup> For heme—peroxidases, the O—O bond-cleavage of hydrogen peroxide was investigated, and a heterolytic mechanism with many similarities to the one described above for cytochrome oxidase was found to be the best one.<sup>75</sup>

Even though the main applications of the present type of model have been made on metal centered redox reactions, several other studies using a similar model have also been performed in our laboratory. For ribonucleotide reductase (RNR), all the steps of the substrate reactions were investigated for both the aerobic and anaerobic classes.<sup>78</sup> A hydrogen atom transfer model for the long-range radical transfer in RNR has also been suggested based on model calculations.<sup>79</sup> All the steps of the still more complicated substrate reaction sequence of copper-containing amine oxidases have furthermore been studied in detail recently.<sup>80</sup> Peptide ring-closing in green fluorescent protein (GFP)<sup>81</sup> and histidine ammonia-lyase<sup>82</sup> have also been investigated. There are also, obviously, many other quantum chemical studies of enzyme reaction mechanisms performed in other laboratories and which are therefore not covered in this review, where similar or rather different theoretical models have been used. It is clear that this field is just in its beginning, and it can safely be predicted that the number of applications will quickly multiply the coming years.

## References and Notes

- (1) Siegbahn, P. E. M. Electronic Structure Calculations for Molecules Containing Transition Metals. In *Adv. Chem. Phys.*; Prigogine, I., Rice, S. A., Eds.; Wiley: New York, 1996; Vol. XCIII, pp 333–387.
- (2) Siegbahn, P. E. M.; Blomberg, M. R. A.; Svensson, M. *Chem. Phys. Lett.* **1994**, *223*, 35. Siegbahn, P. E. M.; Svensson, M.; Boussard, P. J. E. *J. Chem. Phys.* **1995**, *102*, 5377.
- (3) Armentrout P. B.; Kickel B. L. In *Organometallic Ion Chemistry*, Freiser, B. S., Ed.; Kluwer: Dordrecht, 1995; pp 1–45.
- (4) Eller, K.; Schwarz, H. *Chem. Rev.* **1991**, *91*, 1121.
- (5) Weisshaar, J. C. In *Gas-phase Metal Reactions*; Fontijn, A., Ed.; Elsevier: Amsterdam, 1992.
- (6) Blomberg, M. R. A.; Siegbahn, P. E. M.; Svensson, M. *J. Am. Chem. Soc.* **1992**, *114*, 6095.
- (7) Wasserman, E. P.; Morse, C. B.; Bergman, R. G. *Science* **1992**, *255*, 315.
- (8) Becke, A. D. *Phys. Rev.* **1988**, *A38*, 3098.
- (9) Becke, A. D. *J. Chem. Phys.* **1992**, *96*, 2155–2160.
- (10) Becke, A. D. *J. Chem. Phys.* **1992**, *97*, 9173–9177.
- (11) Becke, A. D. *J. Chem. Phys.* **1993**, *98*, 5648–5652.
- (12) Blomberg, M. R. A.; Siegbahn, P. E. M.; Babcock, G. T.; Wikström, M. *J. Inorg. Biochem.* **2000**, *80*, 261–269.
- (13) Blomberg, M. R. A.; Siegbahn, P. E. M.; Babcock, G. T.; Wikström, M. *J. Am. Chem. Soc.* **2000**, *122*, 12848–58.
- (14) Wirstam, M.; Siegbahn, P. E. M. *J. Am. Chem. Soc.* **2000**, *122*, 8539–8547.
- (15) Siegbahn, P. E. M. *J. Inorg. Chem.* **2000**, *39*, 2923–2935.
- (16) Stevens, P. J.; Devlin, F. J.; Chabrowski, C. F.; Frisch, M. J. *J. Phys. Chem.* **1994**, *98*, 11623.
- (17) Lee, C.; Yang, W.; Parr, R. G. *Phys. Rev.* **1988**, *B37*, 785.
- (18) Vosko, S. H.; Wilk, L.; Nusair, M. *Can. J. Phys.* **1980**, *58*, 1200.
- (19) (a) Perdew, J. P.; Wang, Y. *Phys. Rev. B* **1992**, *45*, 13244, (b) Perdew, J. P. In *Electronic Structure of Solids*; Ziesche, P., Eischrig, H., Eds.; Akademie Verlag: Berlin, 1991. (c) Perdew, J. P.; Chevary, J. A.; Vosko, S. H.; Jackson, K. A.; Pederson, M. R.; Singh, D. J.; Fiolhais, C. *Phys. Rev. B* **1992**, *46*, 6671.
- (20) Curtiss, L. A.; Raghavachari, K.; Trucks, G. W.; Pople, J. A. *J. Chem. Phys.* **1991**, *94*, 7221.
- (21) Curtiss, L. A.; Raghavachari, K.; Redfern, R. C.; Rassolov, V.; Pople, J. A. *J. Chem. Phys.* **1998**, *109*, 7764–76.
- (22) Curtiss, L. A.; Raghavachari, K.; Redfern, R. C.; Rassolov, V.; Pople, J. A. *J. Chem. Phys.* **2000**, *112*, 7374–83.
- (23) Bauschlicher, C. W., Jr.; Ricca, A.; Partridge, H.; Langhoff, S. R. In *Recent Advances in Density Functional Methods, Part II*; Chong, D. P., Ed.; World Scientific Publishing Company: Singapore, 1997; p 165.
- (24) Siegbahn, P. E. M.; Blomberg, M. R. A. *Chem. Rev.* **2000**, *100*, 421–437.
- (25) Gardner, K. A.; Mayer, J. M. *Science* **1995**, *269*, 1849. Gardner, K. A.; Mayer, J. M. Private communication, 1996.
- (26) Tomasi, J.; Persico, M. *Chem. Rev.* **1994**, *94*, 2027.
- (27) Wiberg, K. B.; Keith, T. A.; Frisch, M. J.; Murcko, M.; *J. Phys. Chem.* **1995**, *99*, 9072.
- (28) Hay, P. J.; Wadt, W. R. *J. Chem. Phys.* **1985**, *82*, 299.
- (29) Frisch, M. J.; Trucks, G. W.; Schlegel, H. B.; Scuseria, G. E.; Robb, M. A.; Cheeseman, J. R.; Zakrzewski, V. G.; Montgomery, J. A., Jr.; Stratmann, R. E.; Burant, J. C.; Dapprich, S.; Millan, J. M.; Daniels, A. D.; Kudin, K. N.; Strain, M. C.; Farkas, O.; Tomasi, J.; Barone, V.; Cossi, M.; Cammi, R.; Mennucci, B.; Pomelli, C.; Adamo, C.; Clifford, S.; Ochterski, J.; Petersson, G. A.; Ayala, P. Y.; Cui, Q.; Morokuma, K.; Malick, D. K.; Rabuck, A. D.; Raghavachari, K.; Foresman, J. B.; Cioslowski, J.; Ortiz, J. V.; Stefanov, B. B.; Liu, G.; Liashenko, A.; Piskorz, P.; Komaromi, I.; Gomperts, R.; Martin, R. L.; Fox, D. J.; Keith, T.; Al-Laham, M. A.; Peng, C. Y.; Nanayakkara, A.; Gonzalez, C.; Challacombe, M.; Gill, P. M. W.; Johnson, B.; Chen, W.; Wong, M. W.; Andres, J. L.; Head-Gordon, M.; Replogle, E. S.; Pople, J. A.; *Gaussian 98*; Gaussian Inc.: Pittsburgh, PA, 1998.
- (30) *Jaguar 4.0*; Schrödinger: Inc., Portland, OR, 2000.
- (31) Siegbahn, P. E. M.; Blomberg, M. R. A.; Crabtree, R. H. *Theor. Chem. Acc.* **1997**, *97*, 289–300.
- (32) Siegbahn, P. E. M.; Crabtree, R. H. *J. Am. Chem. Soc.* **1997**, *119*, 3103–3113.
- (33) Siegbahn, P. E. M. *J. Comput. Chem.*, in press.
- (34) Siegbahn, P. E. M. *J. Inorg. Chem.* **1999**, *38*, 2880–2889.
- (35) Himio, F.; Eriksson, L. A.; Maseras, F.; Siegbahn, P. E. M. *J. Am. Chem. Soc.* **2000**, *122*, 8031–8036.
- (36) Siegbahn, P. E. M. *Theor. Chem. Acc.* **2001**, *105*, 197–206.
- (37) Siegbahn, P. E. M. Unpublished results, 2000.
- (38) Blomberg, M. R. A.; Siegbahn, P. E. M.; Babcock, G. T. *J. Am. Chem. Soc.* **1998**, *120*, 8812–8824.
- (39) Dismukes, G. C. *Chem. Rev.* **1996**, *96*, 2909–2926.
- (40) Rod, T. H.; Hammer, B.; Nørskov, J. K. *Phys. Rev. Lett.* **1999**, *82*, 4054–4057.
- (41) Noodleman, L.; Li, J.; Zhao, X.-G.; Richardson, W. H. In *Methods in Chemistry and Materials Science*; Springborg, M., Ed.; Wiley: New York, 1997; pp 149–187.
- (42) Yoshikawa, S.; Shinzawa-Itoh, K.; Nakashima, R.; Yaono, R.; Yamashita, E.; Inoue, N.; Yao, M.; Fei, M. J.; Libeu, C. P.; Mizushima, T.; Yamaguchi, H.; Tomizaki, T.; Tsukihara, T. *Science* **1998**, *280*, 1723–1729.
- (43) Ostermeier, C.; Harrenga, A.; Ermler, U.; Michel, H. *Proc. Natl. Acad. Sci. U.S.A.* **1997**, *94*, 10547–10553.
- (44) Roach, P. L.; Clifton, I. J.; Fülöp, V.; Harlos, K.; Barton, G. J.; Hajdu, J.; Andersson, I.; Schofield, C. J.; Baldwin, J. E. *Nature* **1995**, *375*, 700–704.
- (45) Proshlyakov, D. A.; Pressler, M. A.; DeMaso, C.; Leykam, J. F.; DeWitt, D. L.; Babcock, G. T. *Science* **2000**, *290*, 1588–1591.
- (46) Proshlyakov, D. A.; Pressler, M. A.; Babcock, G. T. *Proc. Natl. Acad. Sci. U.S.A.* **1998**, *95*, 8020–25.
- (47) Blomberg, M. R. A.; Siegbahn, P. E. M. Unpublished results, 2000.
- (48) Mitchell, R.; Rich, P. R. *Biochim. Biophys. Acta* **1994**, *1186*, 19–26.
- (49) Baldwin, J. E.; Bradley, M. *Chem. Rev.* **1990**, *90*, 1079–1088.
- (50) Baldwin, J. E.; Lynch, G. P.; Schofield, C. J. *Tetrahedron* **1992**, *48*, 9085–9100.
- (51) Feig, A. L.; Lippard, S. J. *Chem. Rev.* **1994**, *94*, 759–805.
- (52) Que, L., Jr.; Ho, R. Y. N. *Chem. Rev.* **1996**, *96*, 2607–2624.
- (53) Solomon, E. I.; Brunold, T. C.; Davis, M. I.; Kemsley, J. N.; Lee, S.-K.; Lehnert, N.; Neese, F.; Skulan, A. J.; Yang, Y.-S.; Zhou, J. *Chem. Rev.* **2000**, *100*, 235–349.
- (54) Burzlaff, N. I.; Rutledge, P. J.; Clifton, I. J.; Hensgens, C. M. H.; Pickford, M.; Adlington, R. M.; Roach, P. L.; Baldwin, J. E. *Nature* **1999**, *401*, 721–724.
- (55) Wallar, B. J.; Lipscomb, J. D. *Chem. Rev.* **1996**, *96*, 2625–2657.
- (56) Valentine, A. M.; Lippard, S. J. *J. Chem. Soc., Dalton Trans.* **1997**, 3925.
- (57) Rosenzweig, A. C.; Nordlund, P.; Takahara, P. M.; Frederick, C. A.; Lippard, S. J. *Chem. Biol.* **1995**, *2*, 409–418.
- (58) Deighton, N.; Podmore, I. D.; Symons, M. C. R.; Wilkins, P. C.; Dalton, H. *J. Chem. Soc., Chem. Commun.* **1991**, 1086–1088.
- (59) Valentine, A. M.; Le Tadic-Biadatti, M.-H.; Toy, P. H.; Newcomb, M.; Lippard, S. J. *J. Biol. Chem.* **1999**, *274*, 10771–10776 and references therein.
- (60) Basch, H.; Mogi, K.; Musaev, D. G.; Morokuma, K. *J. Am. Chem. Soc.* **1999**, *121*, 7249–7256.
- (61) Siegbahn, P. E. M. *J. Biol. Inorg. Chem.* **2001**, *6*, 27–45.

- (62) Yachandra, V. K.; Sauer, K.; Klein, M. P. *Chem. Rev.* **1996**, *96*, 2927–2950.
- (63) Kok, B.; Forbush, B.; McGloin, M. *Photochem. Photobiol.* **1970**, *11*, 457.
- (64) Barry, B. A.; Babcock, G. T. *Proc. Natl. Acad. Sci. U.S.A.* **1987**, *84*, 7099–7103.
- (65) Babcock, G. T. In *Photosynthesis from Light to Biosphere*; Mathis, P., Ed.; Kluwer: Dordrecht, 1995; Vol 2, p 209.
- (66) Haumann, M.; Junge, W. *Biochim. Biophys. Acta* **1999**, *1411*, 86–91.
- (67) Blomberg, M. R. A.; Siegbahn, P. E. M.; Styring, S.; Babcock, G. T.; Åkermark, B.; Korall, P. *J. Am. Chem. Soc.* **1997**, *119*, 8285–8292.
- (68) Siegbahn, P. E. M.; Crabtree, R. H. *J. Am. Chem. Soc.* **1999**, *121*, 117–127.
- (69) Styring, S. A.; Rutherford, A. W. *Biochemistry* **1988**, *27*, 4915–4923.
- (70) Sharp, R. R. In *Manganese Redox Enzymes*; Pecoraro, V. L., Ed.; VCH: New York, 1992; pp 177–196.
- (71) Messinger, J.; Badger, M.; Wydrzinski, T. *Proc. Natl. Acad. Sci. U.S.A.* **1995**, *92*, 3209–3213.
- (72) Blomberg, M. R. A.; Siegbahn, P. E. M. Unpublished results, 2000.
- (73) Siegbahn, P. E. M.; Svensson, M.; Westerberg, J.; Crabtree, R. H. *J. Phys. Chem. B* **1998**, *102*, 1615–1623.
- (74) Lind, T.; Siegbahn, P. E. M.; Crabtree, R. H. *J. Phys. Chem. B* **1999**, *103*, 1193–1202.
- (75) Wirstam, M.; Blomberg, M. R. A.; Siegbahn, P. E. M. *J. Am. Chem. Soc.* **1999**, *121*, 10178–10185.
- (76) Pavlov, M.; Siegbahn, P. E. M.; Blomberg, M. R. A.; Crabtree, R. H. *J. Am. Chem. Soc.* **1998**, *120*, 548–555. Pavlov, M.; Siegbahn, P. E. M.; Blomberg, M. R. A. *Int. J. Quantum Chem.* **1999**, *73*, 197–207. Siegbahn, P. E. M.; Blomberg, M. R. A.; Wirstam, M.; Crabtree, R. H. *J. Biol. Inorg. Chem.*, in press.
- (77) Pelmenchikov, V.; Blomberg, M. R. A.; Siegbahn, P. E. M. *J. Biol. Inorg. Chem.*, in press.
- (78) Siegbahn, P. E. M. *J. Am. Chem. Soc.* **1998**, *120*, 8417–8429. Himo, F.; Siegbahn, P. E. M. *J. Phys. Chem.* **2000**, *104*, 7502–7509. Cho, K.-B.; Himo, F.; Gräslund, A.; Siegbahn, P. E. M. *J. Phys. Chem. B* **2001**, *105*, 6445–6452.
- (79) Siegbahn, P. E. M.; Blomberg, M. R. A.; Pavlov, M. *Chem. Phys. Lett.* **1998**, *292*, 421–430. Siegbahn, P. E. M.; Eriksson, L.; Himo, F.; Pavlov, M. *J. Phys. Chem. B* **1998**, *102*, 10622–10629.
- (80) Prabhakar, R.; P. E. M. Siegbahn *J. Phys. Chem. B* **2001**, *105*, 4400–08.
- (81) Siegbahn, P. E. M.; Zimmer, M. *Int. J. Quantum Chem.* **2001**, *81*, 169–186.
- (82) Donnelly, M.; Fedeles, F.; Wirstam, M.; Siegbahn, P. E. M.; Zimmer, M. *J. Am. Chem. Soc.* **2001**, *123*, 4679.